Pores Formed by Baxα5 Relax to a Smaller Size and Keep at Equilibrium

Gustavo Fuertes,[†] Ana J. García-Sáez,[‡] Santi Esteban-Martín,[†] Diana Giménez,[†] Orlando L. Sánchez-Muñoz,[†] Petra Schwille,[‡] and Jesús Salgado[†*]

[†]Instituto de Ciencia Molecular, Universidad de Valencia, Paterna, Spain; and [‡]Biotechnologisches Zentrum der Technische Universität Dresden, Dresden, Germany

ABSTRACT Pores made by amphipathic cationic peptides (e.g., antimicrobials and fragments of pore-forming proteins) are typically studied by examining the kinetics of vesicle leakage after peptide addition or obtaining structural measurements in reconstituted peptide-lipid systems. In the first case, the pores have been considered transient phenomena that allow the relaxation of the peptide-membrane system. In the second, they correspond to equilibrium structures at minimum free energy. Here we reconcile both approaches by investigating the pore activity of the α5 fragment from the proapoptotic protein Bax (Baxα5) before and after equilibrium of peptide/vesicle complexes. Quenching assays on suspensions of large unilamellar vesicles suggest that in the presence of Baxα5, the vesicles maintain a leaky state for hours under equilibrium conditions. We proved and analyzed stable pores on single giant unilamellar vesicles (GUVs) in detail by monitoring the entrance of dyes added at different times after incubation with the peptide. When the GUVs came in contact with Baxα5, leakage started stochastically, was delayed for various periods of time, and in the majority of cases proceeded rapidly to completion. After hours in the presence of the peptide, the same individual GUVs that refilled completely at first instance maintained a porated state, which could be observed in subsequent leak-in events for serially added dyes. However, these long-term pores were smaller in size than the initial equilibration pores. Stable pores were also detected in GUVs made in the presence of Baxα5. The latter pores can be considered equilibrium states and may correspond to structures measured previously in bilayer stacks. Although pore formation may occur as a kinetic process, equilibrium pores may also be functionally relevant structures, especially in highly regulated systems such as the apoptotic mitochondrial pores induced by Bax.

INTRODUCTION

Amphipathic cationic polypeptides of varying complexity and functions, including peptide antibiotics (1) and apoptotic Bcl2 proteins (2) or fragments thereof (3–6), interact with lipid membranes and increase their permeability to polar solutes. The mechanisms that lead to membrane leakage are poorly understood (3), but have been described by a variety of models in which an as yet unknown active structure is usually defined as a pore (1,7). The majority of such models are supported by investigations of pore activity, such as kinetic studies of the leakage of fluorescence probes in ensembles of large unilamellar vesicles (LUVs) (8) or individual giant unilamellar vesicles (GUVs) (9,10). The recorded kinetics results from multiple overlapping equilibration processes such as peptide diffusion, binding to the membrane, structural reorganization of the complex, pore formation, and finally the release of the probe. Thus, the activity-based or kinetic models refer essentially to the mechanism of pore formation in close connection to the equilibration of the peptide-vesicle complexes (11,12). The initial binding of the peptide at the interface of the accessible (external) monolayer, called the B_{ex} state (9,13) (Fig. 1 *A*, *left*), is considered to cause mass imbalance and asymmetric area stretching. Above a critical mole fraction of bound peptide, the B_{ex} state evolves cooperatively and stochastically for each individual vesicle into a porated P_i state (9,13). The pores are assumed to be disordered or chaotic structures (13,14), probably related to the so-called toroidal pores (11,15), lined by lipids and peptides (Fig. 1 *A*, *right*), as described by molecular-dynamics simulations (16,17). Such a mechanism is reminiscent of the two-stage process that was recently proposed for the activity of the CM15 antimicrobial peptide on individual bacteria, as studied by high-speed atomic force microscopy (18). Because the leakage kinetics is related to the relaxation of the membrane after a peptide attack, pores are naturally viewed as transient structures (11,12,16,19–21). Nevertheless, in most cases studied, the pores are sufficiently long-lived to allow for complete release of vesicle-entrapped dyes, and are thus said to follow an all-or-none release mechanism (8,9,19,20,22,14).

Although natural peptide-induced pores in cells appear to occur as kinetic processes (18,23), equilibrium pores may also be physiologically relevant (24). Moreover, long-term and equilibrium structures can be important for pores made by proteins such as Bcl-2 family members and bacterial toxins (25), which are complex and highly regulated phenomena and may function as stable assemblies. Another reason to investigate pores at equilibrium is that molecular models cannot be easily deduced from kinetic studies only (8,13,26,27). Structural investigations of peptide-membrane

Submitted May 13, 2010, and accepted for publication August 26, 2010.

*Correspondence: jesus.salgado@uv.es

García-Sáez's present address is Max Planck Institute for Metals Research and German Cancer Research Center, Heidelberg, Germany.

Santi Esteban-Martín's present address is Institute for Research in Biomedicine, Barcelona, Spain.

Editor: Huey W. Huang.

0006-3495/10/11/2917/9 $2.00

doi: 10.1016/j.bpj.2010.08.068

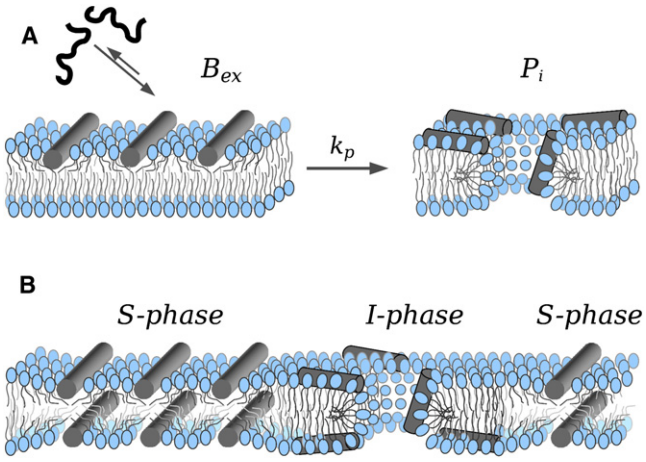

FIGURE 1 Cartoons of kinetic, two-state ($B_{ex} \rightarrow P_i$), and equilibrium two-phase (*S*/*I*) pore models. (*A*) The initial asymmetric binding-refolding of active peptides at the membrane interface (B_{ex} state) drives the transition to a pore P_i state (9,13). (*B*) At equilibrium the peptide is bound interfacially to both monolayers, causing area expansion and membrane thinning (10,30) (*S*-phase). Above a threshold P/L ratio, it coexists with a different molecular organization (7,26) (*I*-phase) corresponding to observable toroidal pores (31). The particular organization of peptides is unknown (the one chosen for this model is arbitrary).

systems have been performed on supported multibilayer stacks made from equilibrated peptide/lipid mixtures. Oriented circular dichroism (28) and NMR (29) reveal a change in the orientation of peptide helices from a flat, *S*, to a tilted/inserted, *I*, alignment, past a threshold peptide/lipid molar ratio, P/L* (7,15,30). These peptide-tilt states (7) were recently reformulated as two phases (26), modeled schematically in Fig. 1 *B*. The *S*-phase corresponds to interfacial binding of the peptide and is accompanied by an increase in the interfacial area (10) and concomitant membrane thinning (30). Because the system is measured at equilibrium and reconstituted from a homogeneous mixture, the peptide should be bound equally to both monolayers. At P/L > P/L*, the *S*-phase coexists with the *I*-phase, and in these conditions stable pores can be detected by neutron and x-ray scattering (15,30). The lipidic outline of toroidal pores induced by an α5 fragment of the apoptotic protein Bax (Baxα5) was recently obtained by x-ray diffraction of bilayer stacks containing brominated lipids (31). The peptide molecules associated to such a lipidic pore were not observed in the x-ray studies, but it was assumed that they bind close to the pore rim and correspond to the tilted peptide state that defines the *I*-phase.

The connection between kinetic and equilibrium pores is unclear, and the relationship between the postulated $B_{ex} \rightarrow P_i$ transition (9,13) and two-phase *S*/*I* model (7,26) remains undefined. Two attempts have been made to correlate kinetic and equilibrium pores. Preequilibrium magainin pores in vesicles, detected by cryo-electron microscopy, were found to be comparable to those studied by neutron scattering in equilibrated bilayer stacks (32). On the other hand, the time-dependent area expansion of single GUVs due to melittin binding was correlated to the membrane thinning observed at equilibrium (10). However, the kinetics of equilibrium pores has not yet been characterized.

Here, we describe vesicle poration by a Baxα5 fragment at long term and under equilibrium. The protein Bax is a critical regulator of physiological cell death in mammals. It controls the release of mitochondrial apoptotic proteins (33), which is believed to proceed through toroidal proteolipidic pores (34,35). The Baxα5 peptide acts as a minimal active fragment that is able to release cytochrome *c* from isolated mitochondria (4). In previous studies, investigators examined slightly longer versions in vesicle leakage experiments out-of-equilibrium and ion channels in black lipid membranes, and concluded that they induce toroidal pores (5,6,36). Reconstituted in different types of supported bilayers, the peptides were observed to exhibit a tilted orientation (5) and reduce the membrane line tension (36). The lipidic structure of peptide-induced toroidal pores was determined by x-ray diffraction (31). Our experiments in LUV suspensions suggested that Baxα5 forms stable pores at equilibrium, and we subsequently proved this through the direct observation of individual GUVs over long periods of time after peptide addition. We propose that the activities of long-term and equilibrium pores reported here correspond to the structures investigated in bilayer stacks, and we demonstrate that these pores differ from preequilibrium kinetic pores at least in terms of size.

MATERIALS AND METHODS

Lipids, fluorescence probes, and peptides

For this study, 1-palmitoyl-2-oleoyl-*sn*-glycero-3-phosphocholine (POPC), 1,2-dioleoyl-*sn*-glycero-3-phosphoethanolamine-*N*-(7-nitro-2-1,3-benzoxadiazol-4-yl) (NBD-PE), and bovine brain cardiolipin (CL) were purchased from Avanti Polar lipids (Alabaster, AL). Calcein, sodium dithionite, and 1,1,1,3,3,3-hexafluoroisopropanol (HFIP) were obtained from Sigma-Aldrich (St. Louis, MO). 1,19-Dioctadecyl-3,3,39,39-tetramethylindodicarbocianin (DiD), Alexa488, Alexa555, and AlexaFluor647 succinimidyl ester were obtained from Molecular Probes/Invitrogen (Eugene, OR). Atto655 was purchased from Atto-Tec (Germany).

Baxα5 encompasses helix 5 of human Bax (37), with sequence WGRVVALFYFASKLVLKALSTK, where Ser-20 substitutes the natural Cys to avoid dimerization. It was synthesized and purified as described previously (5). The unlabeled peptide was acetylated at the N-terminus and amidated at the C-terminus. For the fluorescence-labeled peptide, the N-terminus was kept free and subsequently coupled to Alexa647 succinimidyl ester directly in the synthesis column. Peptide stock solutions were prepared in HFIP to avoid aggregation, and aliquots were diluted in phosphate-buffered saline (PBS) immediately before use to minimize the amount of organic solvent added to the vesicles. Peptide concentrations were determined by UV-Vis absorbance ($\varepsilon_{280} = 6990\ M^{-1}cm^{-1}$).

Leakage assays with LUVs

Calcein release

LUVs with entrapped calcein (80 mM), made of POPC or POPC/CL (80:20), were prepared in PBS using the extrusion method (38). CL was

used because of the suggested significance of this lipid for the function of Bax (39). The excess nonencapsulated dye was removed by exchanging LUVs into fresh PBS through Sephadex-G50 (Sigma-Aldrich) minicolumns. Lipid concentrations were determined with the use of a kit from Wako Chemicals (Japan). Calcein efflux was measured as the relief of self-quenching from the moment of peptide addition (38), using a spectrofluorimeter (Photon Technology International, Japan) with emission at 520 nm and excitation at 480 nm. The percentage of calcein release at time t after peptide addition ($R_t^{\%}$) was calculated from the fluorescence at that time, F_t, with respect to the minimum fluorescence F_i^{min} (before peptide addition) and the maximum fluorescence $F_\infty{}^{max}$ (upon addition of Triton X-100), according to the equation $R_t^{\%} = 100 \times (F_t - F_i^{min})/(F_\infty{}^{max} - F_i^{min})$ (5).

Quenching of labeled lipids

LUVs were prepared in PBS with POPC/NBD-PE (99.5:0.5) or POPC/CL/NBD-PE (79.5:20:0.5) lipids. For vesicles made in the presence of peptide, the Baxα5 and lipids were initially mixed in organic solvent at the amounts required. The quenching assay was carried out according to McIntyre and Sleight (40). LUVs labeled with NBD-PE (0.5 mol%) were diluted in PBS (pH 7.4) to 5 μM lipids in a 1 mL quartz cuvette and mixed with the desired amounts of Baxα5. At defined times after mixing, sodium dithionite was incorporated to a concentration of 20 mM from a 1 M fresh stock in 1 M Tris-HCl, pH 10. This pH is important to stabilize the reactant in the stock, but the small aliquots added did not significantly change the pH in the buffered vesicle suspensions. The fluorescence of NBD-PE was registered with excitation at 470 nm and emission at 540 nm. The quenching at time τ after dithionite addition was calculated as a percentage ($Q_\tau^{\%}$), from the fluorescence at that time, F_τ, with respect to the maximum fluorescence $F_0{}^{max}$ (before dithionite addition) and the minimum fluorescence $F_\infty{}^{min}$ (upon addition of Triton X-100), according to the equation $Q_\tau^{\%} = 100\times(F_0{}^{max} - F_\tau)/(F_0{}^{max} - F_\infty{}^{min})$. For comparison with the results of calcein release, differences between values in the presence ($Q_\tau^{\%,pep}$) and absence ($Q_\tau^{\%,mem}$) of peptide were calculated and expanded to a 0–100% scale as $\Delta Q_\tau^{\%} = 2\times(Q_\tau^{\%,pep} - Q_\tau^{\%,mem})$.

Experiments with single GUVs

POPC/CL GUVs (80:20) were made by electroformation (41). GUVs prepared in the absence of peptide contained the lipophilic dye DiD (0.05%) to allow observation of the membrane (42). For GUVs reconstituted in the presence of peptide, Alexa647-labeled Baxα5 was codissolved with the lipids at the required amounts. The electroformation chamber was filled with a ~300 mM sucrose solution, adjusted to be isoosmolar with PBS from the observation chamber. GUV suspensions were transferred to the observation chamber in the amounts required for ~6 μM lipids. Such a concentration was estimated from measurements in batches of GUVs made in parallel under equal conditions, which were concentrated 10–15 times and analyzed using the kit from Wako Chemicals (Japan).

Confocal microscopy

GUVs were observed at room temperature in multitrack mode on a LSM510 confocal fluorescence microscope using a C-Apochromat 40× 1.2 NA water immersion objective (both from Zeiss, Jena, Germany). For the first track, the excitation light was from Ar-ion (488 nm) and He-Ne (633 nm) lasers and the emission was split into two channels and filtered by a 650 nm long-pass filter (channel 1) and a 505–550 nm band-pass filter (channel 3). For the second track, the sample was excited with an He-Ne laser at 543 nm and the emission light was filtered through a 560–615 nm band-pass filter (channel 2). Images were recorded in grayscale, pseudo-colored red (channel 1), blue (channel 2), or green (channel 3), and processed with the help of ImageJ (http://rsbweb.nih.gov/ij/).

Successive leak-in kinetics

After PBS, Baxα5, and a dye (Alexa555, 1250 Da) were mixed in the observation chamber, an aliquot of sucrose-loaded GUVs was added. The vesicles then sank to the bottom of the chamber, where they were observed. Images were recorded every 10 s and the change in fluorescence intensity inside individual GUVs was analyzed over time. After 2 h, a second dye (Alexa488, 640 Da) was added and the dye entry kinetics was again monitored. A third dye (Atto655, 630 Da) was added ~15 min later and its leak-in kinetics was recorded.

For comparison with successive leak-in events, the volume flux J_v through the vesicle membrane was determined. For the first leakage, the fluorescence inside a GUV at any given time (F_t) was normalized (F_t^N) with respect to the fluorescence at time 0 (F_0) and to the almost constant outside fluorescence (F_t^{out}), according to $F_t^N = (F_t - F_0)/(F_t^{out} - F_0)$. Then, the flux J_v (in μm/min) was obtained from a fit of normalized values to the exponential equation $F_t^N = 1 - e^{-3J_v t/Rt}$ (43), where R is the radius of the vesicle. For the second and third leakages, however, measurements were made just after the dye was added, and the outside concentration of the dye was changed by dilution from the point of addition. In these cases the flux was determined by a fit to the raw fluorescence with the equation $F_t = F_0 + (F_t^{out'} - F_0) \times (1 - e^{-3J_v t/R})$. $F_t^{out'}$ represents the time-dependent outside fluorescence in the immediate surroundings of the vesicle, modeled by a first-order exponential decay as $F_t^{out'} = F_\infty^{out} + F_0^{out} e^{-kt}$, where $F_0{}^{out}$ and $F_\infty{}^{out}$ are the fitted values of the outside fluorescence at time 0 and at equilibrium, respectively, and k is the decay constant of the outside fluorescence. The $F_t^{out'}$ values from the fits were used to normalize the kinetics of second and third dyes (see Fig. S1 in the Supporting Material for details).

RESULTS AND DISCUSSION

Capturing long-term and equilibrium pores in ensembles of LUVs

We performed standard assays of peptide-induced pores in suspensions of LUVs (38) by recording the release of entrapped dyes for only a few minutes after peptide addition (Fig. S2). To capture the activity of pores for long time periods after peptide/vesicle mixing, we first chose to use an indirect approach based on quenching of a fluorescent lipid (0.5% NBD-PE) equally distributed in the two monolayers of vesicle membranes as it is reduced by sodium dithionite (40). In the absence of pores or membrane defects, this reactant permeates slowly through phospholipid membranes (44,45) and quenching mainly affects the external monolayer, reaching ~50% (Fig. S3). However, for leaky membranes the inner monolayer becomes also accessible to dithionite, yielding higher levels of quenching.

The assay must be performed and interpreted with care, since apart from pores, membrane defects and lipid flip-flop may also contribute to increase quenching (44), and such effects can intensify when amphipathic peptides bind to the membrane interface. Another reason for caution is that the quenching kinetics is dominated by the dithionite reaction (44), which is slower than the rate of vesicle leakage (compare Fig. S2 and Fig. S3). However, the rate constant for dithionite reduction may be assumed to be independent of the presence of the peptide, and for a given time after dithionite addition, the increase in quenching with respect to the absence of peptide should be proportional to the increased accessibility of NBD-PE.

The increments of normalized NBD-PE quenching 250 s after dithionite addition ($\Delta Q_{250}^{\%}$; see Materials and Methods) in LUVs preincubated with Baxα5 are represented

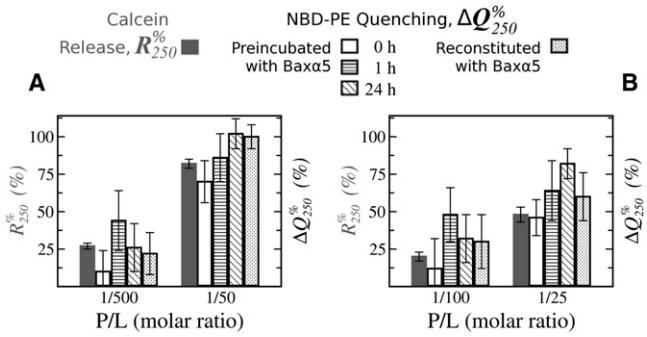

FIGURE 2 Short-term, long-term, and equilibrium pore activities in ensembles in LUVs. (*A*) LUVs of POPC/NBD-PE (99.5:0.5), P/L 1/500 and 1/50. (*B*) POPC/CL/NBD-PE (79.5:20:0.5), P/L 1/100 and 1/25. Both graphs show normalized differences (with peptide, minus without peptide) of percentages of quenching of NBD-PE 250 s after addition of dithionite, $\Delta Q_{250}{}^{\%}$ (see Fig. S3). Baxα5 was either added simultaneously with dithionite (0 h) or preincubated with LUVs for 1 h or 24 h. Alternatively, LUVs were prepared in the presence of the peptide (reconstituted). Percentages of calcein release from LUVs 250 s after peptide addition, $R_{250}{}^{\%}$ (*gray*; see Fig. S2), are also shown for comparison. Within each group of experiments (*A* and *B*), all data correspond to the same batch of all components and experiments were run in a single session. Bars correspond to averages of three repetitions ± the SD.

in Fig. 2 for two lipid compositions, each at two P/L ratios. When Baxα5 and dithionite were added simultaneously to either POPC/NBD-PE (99.5:0.5) or POPC/CL/NBD-PE (79.5:20:0.5; Fig. 2, *A* and *B*, respectively, *white bars*), there was an increment of quenching ($\Delta Q_{250}{}^{\%} > 0$) compared to LUVs in the absence of peptide, indicating that NBD-PE from the internal monolayer was accessible to dithionite. The extent of $\Delta Q_{250}{}^{\%}$ was comparable, within error, to the calcein release ($R_{250}{}^{\%}$) observed under analogous conditions (Fig. 2, *A* and *B*, *gray bars*), and, of importance, the P/L dependence was very similar for the two types of experiments. In addition, both $R_{250}{}^{\%}$ and $\Delta Q_{250}{}^{\%}$ decreased comparably in the presence of CL, as expected from previous studies (5). Altogether, these data indicate that under our conditions the extra accessibility of dithionite to internal monolayer lipids in the presence of Baxα5 is due to peptide-induced membrane permeability and/or to phenomena closely coupled to the presence of pores.

The NBD-PE quenching experiment on vesicles previously incubated with Baxα5 allowed us to register vesicle permeability at any stage of an evolved peptide/membrane system. The results in Fig. 2, *A* and *B* (*striped bars*), show that the vesicle leaky state was still present at least 24 h after addition of the peptide. Because the relaxation of initial pore states may be slow, we repeated the experiments using vesicles reconstituted with Baxα5 (Fig. 2, *A* and *B*, *dotted bars*). Again, the values of $\Delta Q_{250}{}^{\%}$ suggest that pores also exist in this truly equilibrated system. The quenching levels are similar for long-term incubated and reconstituted Baxα5/LUVs, and they all are larger than the values obtained without preincubation with Baxα5; however, these and other small differences may not be significant, considering the error of the experiments. The dose-response and lipid-composition effects of long-term and equilibrium activities were basically maintained as described above, suggesting that they were due to peptide-induced pores. In the next section we demonstrate the existence of such pores in single GUVs by direct visualization of leakage using fluorescence microscopy.

Successive leakage in single GUVs

The pore activity of peptides and proteins in individual GUVs can be followed with the use of optical microscopy techniques (9,10,46,43). By recording the internalization of fluorescent dyes in selected GUVs (43), these methods also allow multiple leakage events to be monitored at specific moments on the same set of vesicles. We use such a strategy to investigate the permeability of vesicle membranes at short and long times after they come in contact with the peptide, presenting the GUVs with successively added external dyes. The vesicle integrity is controlled by the fluorescence of the inert lipophilic dye (DiD) present in the membrane (42).

In a typical series of experiments (Fig. 3), a suspension of GUVs labeled with DiD (*red*) was added to the observation chamber containing the first dye (Alexa555; Fig. 3 *A*, *blue*) and Baxα5. Vesicle poration then began in a stochastic way, in similarity to previous observations regarding the kinetics of dye release in the presence of magainin 2 (9,13), dye entrance in the presence of the protein equinatoxin II (43), and the kinetics of area/volume vesicle expansion induced by melittin (10). The onset of Baxα5-dependent dye entrance occurred at various times, mostly between 30 min and 1 h (see some examples in Fig. 3 *E*, *left*). However, as soon as it started, the dye concentration reached near-complete equilibration with the outside pool in ~2 min. It was previously observed that the kinetics of accumulating leaky vesicles registered for large ensembles of GUVs from the moment of peptide addition is similar to the kinetics of contents release from LUV suspensions (9,13,43). In both types of ensembles, the kinetics corresponds to the onset of pores in the complete vesicle pool, which at the end point affects a number of vesicles depending on P/L. Two hours after peptide addition (Fig. 3 *B*), all vesicles appear to be intact, but whereas some are completely refilled with Alexa555 (marked in the image of the red channel), others are empty of fluorescence probe. In most refilled vesicles the exchange of contents was complete, and thus it is clear that they followed an all-or-none poration mechanism (8,22,47). However, a few vesicles refilled only partially with dye, because the rate of entrance was very slow and eventually faded away (see Fig. S4 and below). Such behavior corresponds to what is known as graded leakage (8,22,48).

After 2 h of peptide/vesicle equilibration, a second dye was added (Alexa488, *green*), whose leak-in is shown in

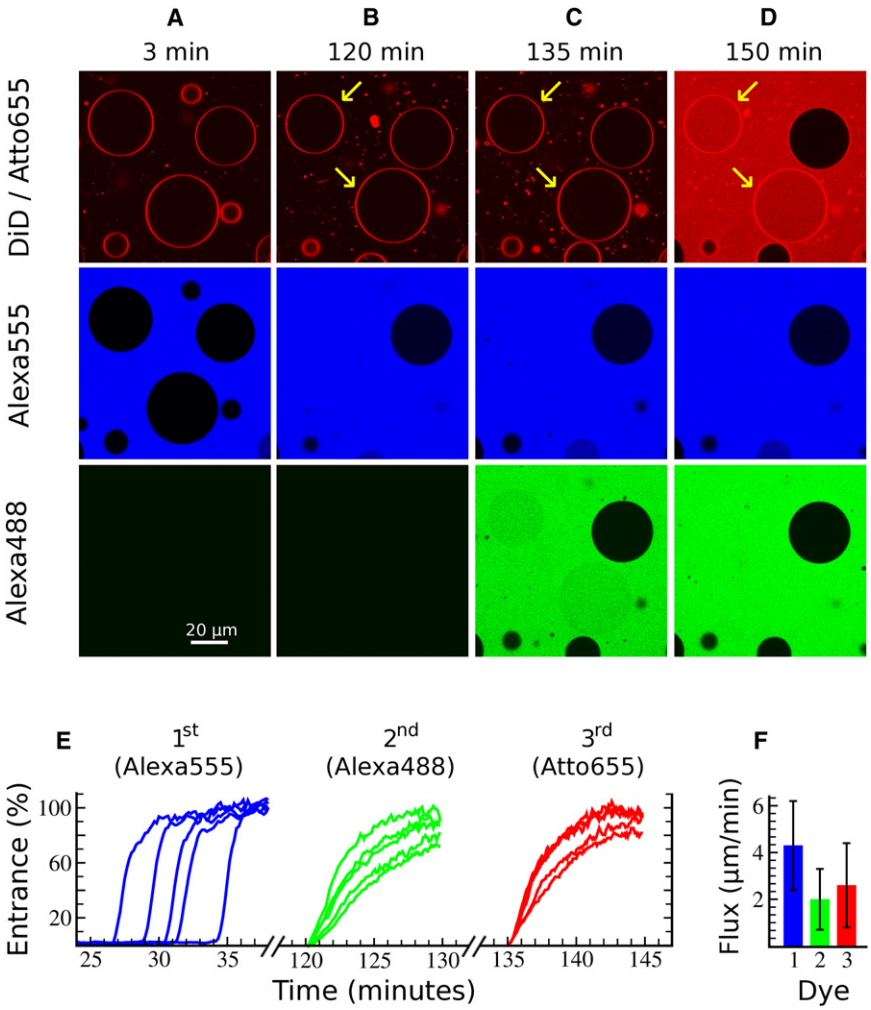

FIGURE 3 Successive leak-in of serially added dyes for individual GUVs. Baxα5 and the first dye (Alexa555, *blue*) are initially present in the observation chamber, where GUVs labeled with DiD (*red*) are added to P/L = 1/90 (time = 0). (*A*) Fluorescence images were recorded starting from minute 3 in three channels. Eventually some GUVs became permeable stochastically and the dye internalized rapidly. Examples of normalized kinetics for five single GUVs are shown in *E* (*left*). (*B*) Two hours later, all GUVs have maintained their integrity (*red*), but some (marked with *arrows*) have allowed complete entrance of the first dye (compare *red* and *blue channels*). Immediately afterward, a second dye (Alexa488, *green*) was added. The same GUVs as before are still permeable but now refill with the second dye at slower rates (*E*, *middle*). (*C*) Images after entrance of the second dye. The leaky vesicles for this dye (*green*) are the same as those for the first dye (*blue*), marked in the image of the red channel. Immediately afterward, a third dye (Atto655, *red*) is added and its entrance is monitored (*E*, *right*). (*D*) Images taken at 150 min show that the porated vesicles are still the same as with the first and second dyes. (*E*) The influx kinetics for the second and third dyes are normalized as explained in Fig. S1. (*F*) Averaged volume fluxes for 40 GUVs ± SD.

pictures taken 15 min later (Fig. 3 *C*). Finally, we added a third dye (Atto655, *red*), and the response can be seen in pictures taken again 15 min later (Fig. 3 *D*). During this time (150 min in total) we registered the fluorescence from the same sets of GUVs. The recorded tracks for the second and third leak-in events, after a careful analysis accounting for the influence of the diffusive equilibration of the dyes (Fig. S1), show that the kinetics are slower than those of the first leakage (Fig. 3 *E*). For a quantitative comparison we fit the leak-in kinetics to exponential functions (43) relating the increase of fluorescence within the porated GUVs to their measured radius (R) and to the volume flux of the probe (J_v; see Materials and Methods, and Fig. S1). Fits of kinetic traces for a total of 40 GUVs yielded average flux values for the second (2.0 ± 1.3 μm/min) and third (2.6 ± 1.8 μm/min) dyes that were smaller than those for the first dye (4.3 ± 1.9 μm/min; Fig. 3 *F*). In addition, we made two clear and remarkable observations:

1. For all leaky vesicles, the entrance of the second and third dyes started with no significant delay, showing that all porated vesicles were already in that state at the moment these dyes were added.
2. All of these porated vesicles were individual vesicles that were completely permeable to the first dye. Additionally, all vesicles that were initially nonpermeable to the first dye remained sealed for the second and third dyes, and the few vesicles that exhibited partial first dye entrance showed no entrance of successive dyes (Fig. S4).

The numbers of tracked vesicles and porated and nonporated vesicles for each dye and for three P/L ratios are given in Table S1. For small P/L cases, there is a fraction of vesicles showing partial or graded first-dye exchange (~22% of all porated for P/L = 1/720) and eventually pore closure (Fig. S4 *E*), i.e., graded leakage appears to be a kinetic mechanism that is linked to peptide/membrane equilibration. On the other hand, the fact that graded filling and all-or-none filling coexist during the equilibration process shows that both mechanisms can occur simultaneously for a given peptide/lipid system, as previously suggested (49). It should also be noted that the vesicle pool contains an intrinsic, small percentage of porated vesicles (~8%) in

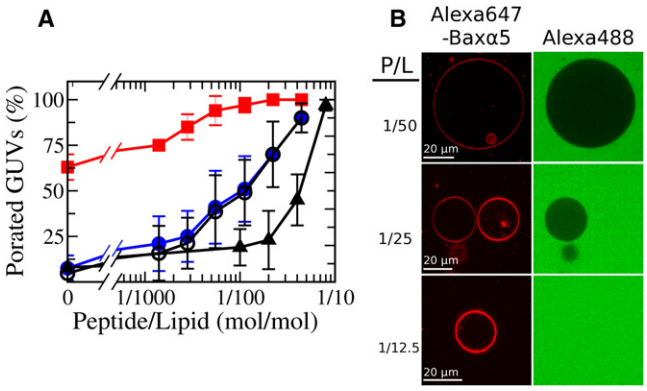

FIGURE 4 P/L dependence of Baxα5 poration on GUVs, and Baxα5 binding and activity in reconstituted systems. (*A*) Dose-response graphs for the leak-in of externally added dyes. The open circles are percentages of GUVs that were permeable to the first dye (Alexa488) during the first 2 h after they came in contact with Baxα5 (including completely and partially filled GUVs); the dose-response curve for any successive dye entrance is slightly different (*solid circles*). The percentage of completely permeable GUVs in the first leakage event, relative to the total permeable GUVs (including partially porated), is represented by squares. Triangles indicate data for the entrance of external Alexa488 at equilibrium, measured with GUVs prepared in the presence of Alexa647-labeled Baxα5. Images of the latter GUVs for three P/L ratios are shown in *B*, demonstrating accumulation of the Alexa647-Baxα5 peptide in the membrane (*left column*) and peptide-induced leakage of Alexa488 (*right column*). See also controls in Fig. S5.

the absence of peptide that exhibit both all-or-none and graded filling (Table S1 and values at P/L = 0 in Fig. 4 *A*), suggesting that at least for the lipid composition used here, the coexistence of both types of mechanisms is a characteristic of lipidic pores.

We also analyzed the dependence of the proportion of Baxα5 porated GUVs on P/L. Plotted using all porated vesicles for the leak-in of the first dye up to the first 2 h (Fig. 4 *A*, *open circles*), the dose-response graph is similar to that measured in calcein-release assays using LUV suspensions (5). Because a few such vesicles (exhibiting graded filling) did not remain in the porated state, the plots for successive dye entrances are slightly different (Fig. 4 *A*, *solid circles*). The number of partially (transiently) porated vesicles also depends on P/L. Thus, from the data of the first leakage event we can also plot the percentage of stably porated vesicles relative to the total number of porated vesicles (stable and transient), which reaches 100% near P/L = 1/100 (Fig. 4 *A*, *squares*). The latter P/L ratio appears reminiscent of threshold values reported in previous studies of other systems (10,13,30,31), and they are also of a similar magnitude.

Pores in reconstituted GUVs

A difference between LUVs and GUVs is that the latter type of vesicles, of much larger size, tends to be more fragile. Thus, to avoid artifacts, leakage events on GUVs were not registered at very long times after they came in contact with the peptide. Instead, as we also did with LUVs, we prepared equilibrated systems by reconstituting GUVs in the presence of Baxα5. Additionally, for these samples we used a fluorescence-labeled version of the peptide (Alexa647-Baxα5) that allowed us to directly test membrane binding. The bright fluorescence of the membrane in the presence of Alexa647-Baxα5 (Fig. 4 *B*, *left*), compared with the weak signal in the presence of Alexa647 alone (control experiment, Fig. S5 *A*), shows peptide binding to the bilayer. Furthermore, the permeabilizing activity of the labeled peptide on single GUVs is comparable to that of the unlabeled peptide (Fig. S5 *B*). The yield of GUV formation in the presence of Alexa647-Baxα5 was low, and the distribution of the peptide among individual vesicles within the same batch was found to be inhomogeneous (see middle image in Fig. 4 *B*, *left*). After addition of Alexa488, internalization of the dye was observed for a fraction of the vesicles that increased with the bulk P/L (Fig. 4 *B*, *right*). The leakage was always of the all-or-none type, again indicating that graded leakage corresponds to equilibration. A dose-response plot for bulk P/L values (Fig. 4 *A*, *triangles*) suggests a threshold P/L for the onset of equilibrium pores near 1/25, which is larger than that extracted from the trend of peptide-added systems (~1/100). We recall that the activity registered with reconstituted LUVs also tends to be smaller than that measured after a few hours in the presence of peptide (Fig. 2). This may indicate that the peptide-added systems were still not equilibrated after 2 h of incubation with the peptide, although we are cautious about this comparison because of the differences between the two types of samples.

Up to this point, we are characterizing leaky or pore states of vesicles more than individual pores. We may by now conclude that the vesicle pore state acquired through equilibration, both in GUVs and LUVs, either maintains or transforms into a long-term and eventually stable (equilibrium) pore state. There also seems to be a threshold P/L value for the onset of both types of pores, which is probably larger at equilibrium, but below saturation, porated and nonporated vesicles coexist and stay in stable or metastable states that do not exchange appreciably among each other.

Kinetic and long-term pores differ at least in size

An important question is, do the initial (kinetic or out-of-equilibrium) pores have properties similar to those observed at long term? Although this is difficult to answer, we addressed it by testing the entry of dyes of different sizes and at different times after incubation with Baxα5. For this purpose, we compared the entrance of Alexa555 (1.25 KDa) and a ~10 KDa calcein-labeled dextran (FD10). FD10 has a hydrodynamic radius of 2.3 nm (50), which is slightly larger than the ~1.7 nm of the physiologically relevant cytochrome *c* (51). Two hours after gently mixing a suspension of GUVs with both dyes and Baxα5, we saw that any chosen

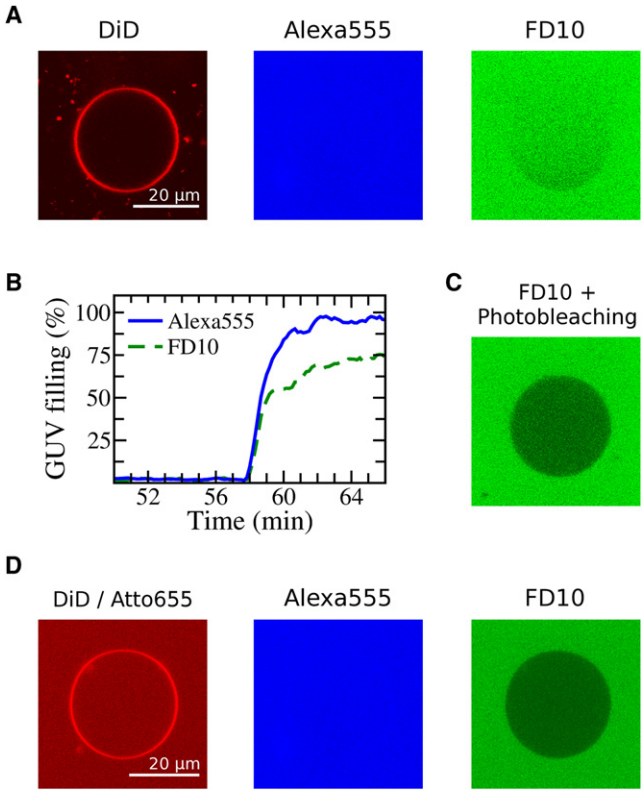

FIGURE 5 Pores shrink with equilibration. (*A*) Example GUV (labeled with DiD, *left*) 2 h after mixing in a solution containing Baxα5, Alexa555 (*middle*), and fluorescence-dextran FD10 (*right*). (*B*) Both dyes leak into the vesicle, starting simultaneously and proceeding at similar rates. However, for FD10 (*dashed*) the communication with the external pool slowed down at some time point and eventually stopped before complete filling occurred. (*C*) Continuing irradiation at 488 nm for 2 min bleached the FD10 fluorescence only from the inside of the GUV. (*D*) In a separate experiment, DiD-labeled GUVs were first put in a solution with Baxα5 and Atto655 to identify GUVs porated at short times (*left*). Two hours later, Alexa555 and FD10 were added together and the vesicles were observed. Vesicles that initially were completely permeable to Atto655 (as in the example shown) were subsequently also fully permeable to Alexa555 (*middle*) but not to FD10 (*right*). The experiments correspond to a bulk P/L of 1/22.5.

individual GUV that was permeable for the Alexa dye (Fig. 5 *A*, *middle*) had also allowed entry of FD10 (Fig. 5 *A*, *right*). As explained above, for a given vesicle the onset of the porated state is normally delayed and stochastic. A recording of the kinetics (Fig. 5 *B*) shows that both fluorescence molecules start entering into the same vesicles simultaneously and initially at a very similar rate. However, whereas the entry of Alexa proceeds smoothly up to complete equilibration with the external pool, the entry of FD10 is slowed down near the end of the kinetics (compare *solid* and *dashed lines* in Fig. 5 *B*). This indicates that although the pores initially were sufficiently large to allow entry of FD10, they relaxed to a smaller size in a few minutes. In fact, we observed that continued irradiation bleached the fluorescence of FD10 only from the inside of the GUV (Fig. 5 *C*), indicating that FD10 had become entrapped and could no longer reequilibrate with the outside pool. To confirm the smaller size of long-term pores, in an independent experiment we monitored the entry of Alexa555 and FD10 added simultaneously to a GUV suspension that was previously incubated with Baxα5 for 2 h. Initially porated GUVs, distinguishable by the complete entrance of Atto655 (present in the external solution from the beginning; Fig. 5 *D*, *left*), allowed immediate and complete entry of added Alexa555 (Fig. 5 *D*, *middle*). However, the same GUVs were very weakly permeable to FD10, which was found to penetrate only to ~12% even 30 min after addition (Fig. 5 *D*, *right*). Considering the approximate size of FD10, we can estimate that the initial pores have a diameter that is clearly larger than ~4.6 nm (6), but they shrink as they relax to a diameter smaller than (but probably not far from) ~4.6 nm.

Pore shrinkage is in agreement with the significantly smaller dye flux found in successive leakage events (Fig. 3, *E* and *F*). A reduction in size after an initial burst was also previously observed for purely lipidic pores induced by tension, which typically relaxed until they closed (52). However, although Baxα5-induced pores start reducing in size quickly after they form, the peptide stabilizes them, avoiding complete closure. On the basis of a kinetic analysis, it was also suggested that the pores formed by melittin shrink with equilibration (27). Such observations can be related to a general role of amphipathic peptides in the stabilization of lipidic pores, as proposed on the basis of theoretical arguments (53) and other single-vesicle experiments (10).

Our data in the case of Baxα5 provide further evidence that preequilibrium and equilibrium pores, although likely related, are not identical. Preequilibrium pores can be seen as a response of the membrane to peptide adsorption in the accessible monolayer. A molecular mechanism for such a situation has been proposed on the basis of molecular-dynamics simulations (16). The increased interfacial area creates a tension that makes the membrane rupture. In principle, this should occur simply above a certain limit of tension, related to a limit of area stress and a limit of bound peptide per unit area. However, in an asymmetrically expanded bilayer, the packing of the compressed monolayer is expected to significantly increase the activation energy for membrane rupture (54). In such a strained metastable state, pores initiate stochastically at points of nucleation of defects. On the other hand, pore formation can generally be assisted by molecules perturbing the packing of the lipids (52,54), in which membrane-adsorbing peptides should also play a role. The onset of peptide-induced pores must be accompanied by a reorganization of the peptide-membrane complex. In turn, the preequilibrium pores themselves may help equilibration of the peptide across the bilayer, as observed in other cases such as magainin 2 and melittin (12,27). However, as the mass imbalance dissipates, the pores of the all-or-none type do not close as is frequently

assumed. Instead, they relax into stable structures that are at least smaller than the preequilibrium pores. It is reasonable to speculate that the stable pores would also be more organized structures.

Finally, an interesting issue is the relevance of equilibrium pores versus kinetic or preequilibrium pores. Other peptides that follow an all-or-none mechanism, such as magainin (20) and cecropin (14), may also form stable pores at equilibrium. On the other hand, peptides that display a graded kinetics of leakage (48) can be expected to form mainly transient pores. From a practical point of view, the structure of transient preequilibrium pores is difficult, if not impossible, to characterize. Not surprisingly, the structural information that is normally available corresponds to equilibrated peptide-membrane complexes. Additionally, from a physiological point of view, it is likely that the function of membrane-active peptides occurs mainly through preequilibrium pores. The fact that the action of antimicrobial peptides on individual bacteria appears to be delayed and stochastic (18), in a manner similar to the action over single vesicles, supports this hypothesis. This is less clear for the case of pore-forming proteins, where the process is mechanistically more complex and regulated, and may need to extend to longer times or involve different steps. In this sense, despite the simplicity of the Baxα5 fragment, the stable pores reported here may well be mechanistically relevant for the function of the full-length protein (55,56). Although they are still not well characterized, the pores formed by the protein Bax are likely stable and organized structures (57,55), and this work shows that the short sequence of the α5 fragment codifies the necessary information to induce and stabilize pores, at least in POPC and POPC/CL membranes. This would be a specific property of this domain of Bax, in comparison with equivalent fragments of other Bcl-2 proteins of a different type (4), that has been selected through evolution to contribute to the function of Bax.

CONCLUSIONS

In summary, this study shows that the Baxα5 peptide in POPC and POPC/CL membranes induces and stabilizes long-lived pores that exist at equilibrium in both suspensions of LUVs and individual GUVs. These pores appear to be mechanistically related to preequilibrium pores, as the first ones are formed in the same vesicles after relaxation of the second. However, the equilibrium pores differ from kinetic pores at least in size, since they exhibit a detectable shrinkage in diameter, suggesting that they may correspond to a different structural organization of the peptide-lipid complexes.

SUPPORTING MATERIAL

One table and five figures with statistical details about the analyzed GUVs (Table S1), quantitative analysis of dye entrance kinetics in GUVs (Fig. S1), kinetics of calcein release (Fig. S2) and quenching of NBD-PE lipids in LUVs (Fig. S3), successive leak-in kinetics in GUVs (Fig. S4), and control experiments for GUVs reconstituted with labeled Bax-a5 are available at http://www.biophysj.org/biophysj/supplemental/S0006-3495(10)01086-6.

This work was supported by the Ministerio de Ciencia e Innovacion (BFU200767097, financed in part by the European Regional Development Fund). G.F. received a grant from the University of Valencia (V-Segles), and A.J.G.-S. was supported by a fellowship from the Max Planck Society.

REFERENCES

1. Zasloff, M. 2002. Antimicrobial peptides of multicellular organisms. *Nature.* 415:389–395.
2. García-Sáez, A. J., G. Fuertes, …, J. Salgado. 2010. Permeabilization of the outer mitochondrial membrane by Bcl-2 proteins. *Adv. Exp. Med. Biol.* 677:91–105.
3. Fuertes, G., D. Giménez, …, J. Salgado. 2010. Role of membrane lipids for the activity of pore forming peptides and proteins. *Adv. Exp. Med. Biol.* 677:31–55.
4. Guillemin, Y., J. López, …, A. Aouacheria. 2010. Synthetic peptides derived from pro- and anti-apoptotic BCL-2 family members have distinct membrane behaviour reflecting functional divergence. *PLoS ONE.* 5:e9066.
5. García-Sáez, A. J., M. Coraiola, …, J. Salgado. 2005. Peptides derived from apoptotic Bax and Bid reproduce the poration activity of the parent full-length proteins. *Biophys. J.* 88:3976–3990.
6. García-Sáez, A. J., M. Coraiola, …, J. Salgado. 2006. Peptides corresponding to helices 5 and 6 of Bax can independently form large lipid pores. *FEBS J.* 273:971–981.
7. Huang, H. W. 2000. Action of antimicrobial peptides: two-state model. *Biochemistry.* 39:8347–8352.
8. Almeida, P. F., and A. Pokorny. 2009. Mechanisms of antimicrobial, cytolytic, and cell-penetrating peptides: from kinetics to thermodynamics. *Biochemistry.* 48:8083–8093.
9. Tamba, Y., and M. Yamazaki. 2005. Single giant unilamellar vesicle method reveals effect of antimicrobial peptide magainin 2 on membrane permeability. *Biochemistry.* 44:15823–15833.
10. Lee, M. T., W. C. Hung, …, H. W. Huang. 2008. Mechanism and kinetics of pore formation in membranes by water-soluble amphipathic peptides. *Proc. Natl. Acad. Sci. USA.* 105:5087–5092.
11. Matsuzaki, K., O. Murase, …, K. Miyajima. 1996. An antimicrobial peptide, magainin 2, induced rapid flip-flop of phospholipids coupled with pore formation and peptide translocation. *Biochemistry.* 35:11361–11368.
12. Matsuzaki, K., O. Murase, …, K. Miyajima. 1995. Translocation of a channel-forming antimicrobial peptide, magainin 2, across lipid bilayers by forming a pore. *Biochemistry.* 34:6521–6526.
13. Tamba, Y., and M. Yamazaki. 2009. Magainin 2-induced pore formation in the lipid membranes depends on its concentration in the membrane interface. *J. Phys. Chem. B.* 113:4846–4852.
14. Gregory, S. M., A. Cavenaugh, …, P. F. Almeida. 2008. A quantitative model for the all-or-none permeabilization of phospholipid vesicles by the antimicrobial peptide cecropin A. *Biophys. J.* 94:1667–1680.
15. Ludtke, S. J., K. He, …, H. W. Huang. 1996. Membrane pores induced by magainin. *Biochemistry.* 35:13723–13728.
16. Sengupta, D., H. Leontiadou, …, S. J. Marrink. 2008. Toroidal pores formed by antimicrobial peptides show significant disorder. *Biochim. Biophys. Acta.* 1778:2308–2317.
17. Leontiadou, H., A. E. Mark, and S. J. Marrink. 2006. Antimicrobial peptides in action. *J. Am. Chem. Soc.* 128:12156–12161.
18. Fantner, G. E., R. J. Barbero, …, A. M. Belcher. 2010. Kinetics of antimicrobial peptide activity measured on individual bacterial cells using high-speed atomic force microscopy. *Nat. Nanotechnol.* 5:280–285.

19. Rathinakumar, R., and W. C. Wimley. 2008. Biomolecular engineering by combinatorial design and high-throughput screening: small, soluble peptides that permeabilize membranes. *J. Am. Chem. Soc.* 130: 9849–9858.
20. Gregory, S. M., A. Pokorny, and P. F. F. Almeida. 2009. Magainin 2 revisited: a test of the quantitative model for the all-or-none permeabilization of phospholipid vesicles. *Biophys. J.* 96:116–131.
21. Rex, S., and G. Schwarz. 1998. Quantitative studies on the melittin-induced leakage mechanism of lipid vesicles. *Biochemistry.* 37:2336–2345.
22. Parente, R. A., S. Nir, and F. C. Szoka, Jr. 1990. Mechanism of leakage of phospholipid vesicle contents induced by the peptide GALA. *Biochemistry.* 29:8720–8728.
23. Imura, Y., N. Choda, and K. Matsuzaki. 2008. Magainin 2 in action: distinct modes of membrane permeabilization in living bacterial and mammalian cells. *Biophys. J.* 95:5757–5765.
24. Mangoni, M. L., N. Papo, …, A. C. Rinaldi. 2004. Effects of the antimicrobial peptide temporin L on cell morphology, membrane permeability and viability of *Escherichia coli*. *Biochem. J.* 380:859–865.
25. Anderluh, G., and J. H. Lakey. 2008. Disparate proteins use similar architectures to damage membranes. *Trends Biochem. Sci.* 33:482–490.
26. Huang, H. W. 2009. Free energies of molecular bound states in lipid bilayers: lethal concentrations of antimicrobial peptides. *Biophys. J.* 96:3263–3272.
27. Matsuzaki, K., S. Yoneyama, and K. Miyajima. 1997. Pore formation and translocation of melittin. *Biophys. J.* 73:831–838.
28. Wu, Y., H. W. Huang, and G. A. Olah. 1990. Method of oriented circular dichroism. *Biophys. J.* 57:797–806.
29. Glaser, R. W., C. Sachse, …, A. S. Ulrich. 2005. Concentration-dependent realignment of the antimicrobial peptide PGLa in lipid membranes observed by solid-state 19F-NMR. *Biophys. J.* 88:3392–3397.
30. Ludtke, S., K. He, and H. Huang. 1995. Membrane thinning caused by magainin 2. *Biochemistry.* 34:16764–16769.
31. Qian, S., W. Wang, …, H. W. Huang. 2008. Structure of transmembrane pore induced by Bax-derived peptide: evidence for lipidic pores. *Proc. Natl. Acad. Sci. USA.* 105:17379–17383.
32. Han, M., Y. Mei, …, S. J. Ludtke. 2009. Characterization of antibiotic peptide pores using cryo-EM and comparison to neutron scattering. *Biophys. J.* 97:164–172.
33. Danial, N. N., and S. J. Korsmeyer. 2004. Cell death: critical control points. *Cell.* 116:205–219.
34. Basañez, G., A. Nechushtan, …, R. J. Youle. 1999. Bax, but not Bcl-xL, decreases the lifetime of planar phospholipid bilayer membranes at subnanomolar concentrations. *Proc. Natl. Acad. Sci. USA.* 96: 5492–5497.
35. Terrones, O., B. Antonsson, …, G. Basañez. 2004. Lipidic pore formation by the concerted action of proapoptotic BAX and tBID. *J. Biol. Chem.* 279:30081–30091.
36. García-Sáez, A. J., S. Chiantia, …, P. Schwille. 2007. Pore formation by a Bax-derived peptide: effect on the line tension of the membrane probed by AFM. *Biophys. J.* 93:103–112.
37. Suzuki, M., R. J. Youle, and N. Tjandra. 2000. Structure of Bax: coregulation of dimer formation and intracellular localization. *Cell.* 103:645–654.
38. Dalla Serra, M., and G. Menestrina. 2003. Liposomes in the study of pore-forming toxins. *Methods Enzymol.* 372:99–124.
39. Kuwana, T., M. R. Mackey, …, D. D. Newmeyer. 2002. Bid, Bax, and lipids cooperate to form supramolecular openings in the outer mitochondrial membrane. *Cell.* 111:331–342.
40. McIntyre, J. C., and R. G. Sleight. 1991. Fluorescence assay for phospholipid membrane asymmetry. *Biochemistry.* 30:11819–11827.
41. Dimitrov, D., and M. Angelova. 1988. Lipid swelling and liposome formation mediated by electric fields. *Bioelectrochem. Bioenerg.* 19:323–336.
42. Kahya, N., D. Scherfeld, …, P. Schwille. 2004. Lipid domain formation and dynamics in giant unilamellar vesicles explored by fluorescence correlation spectroscopy. *J. Struct. Biol.* 147:77–89.
43. Schön, P., A. J. García-Sáez, …, P. Schwille. 2008. Equinatoxin II permeabilizing activity depends on the presence of sphingomyelin and lipid phase coexistence. *Biophys. J.* 95:691–698.
44. Moreno, M. J., L. M. Estronca, and W. L. Vaz. 2006. Translocation of phospholipids and dithionite permeability in liquid-ordered and liquid-disordered membranes. *Biophys. J.* 91:873–881.
45. Langner, M., and S. W. Hui. 1993. Dithionite penetration through phospholipid bilayers as a measure of defects in lipid molecular packing. *Chem. Phys. Lipids.* 65:23–30.
46. Ambroggio, E. E., F. Separovic, …, L. A. Bagatolli. 2005. Direct visualization of membrane leakage induced by the antibiotic peptides: maculatin, citropin, and aurein. *Biophys. J.* 89:1874–1881.
47. Weinstein, J. N., R. D. Klausner, …, R. Blumenthal. 1981. Phase transition release, a new approach to the interaction of proteins with lipid vesicles. Application to lipoproteins. *Biochim. Biophys. Acta.* 647:270–284.
48. Yandek, L. E., A. Pokorny, …, P. F. Almeida. 2007. Mechanism of the cell-penetrating peptide transportan 10 permeation of lipid bilayers. *Biophys. J.* 92:2434–2444.
49. Ladokhin, A. S., W. C. Wimley, and S. H. White. 1995. Leakage of membrane vesicle contents: determination of mechanism using fluorescence requenching. *Biophys. J.* 69:1964–1971.
50. Sanders, S. E., J. L. Madara, …, S. P. Colgan. 1995. Assessment of inflammatory events in epithelial permeability: a rapid screening method using fluorescein dextrans. *Epithelial Cell Biol.* 4:25–34.
51. Mirkin, N., J. Jaconcic, …, A. Moreno. 2008. High resolution X-ray crystallographic structure of bovine heart cytochrome *c* and its application to the design of an electron transfer biosensor. *Proteins.* 70:83–92.
52. Karatekin, E., O. Sandre, …, F. Brochard-Wyart. 2003. Cascades of transient pores in giant vesicles: line tension and transport. *Biophys. J.* 84:1734–1749.
53. Huang, H. W., F. Y. Chen, and M. T. Lee. 2004. Molecular mechanism of peptide-induced pores in membranes. *Phys. Rev. Lett.* 92:198304.
54. Esteban-Martín, S., H. J. Risselada, J. Salgado, and S. J. Marrink. 2009. Stability of asymmetric lipid bilayers assessed by molecular dynamics simulations. *J. Am. Chem. Soc.* 131:15194–15202.
55. Bleicken, S., M. Classen, …, E. Bordignon. 2010. Molecular details of Bax activation, oligomerization, and membrane insertion. *J. Biol. Chem.* 285:6636–6647.
56. Schafer, B., J. Quispe, …, T. Kuwana. 2009. Mitochondrial outer membrane proteins assist Bid in Bax-mediated lipidic pore formation. *Mol. Biol. Cell.* 20:2276–2285.
57. Epand, R. F., J. C. Martinou, …, C. M. Yip. 2002. Direct evidence for membrane pore formation by the apoptotic protein Bax. *Biochem. Biophys. Res. Commun.* 298:744–749.